POLITECNICO DI TORINO
Repository ISTITUZIONALE

Mitigation of Crowd-Induced Vibrations in Historic Masonry Towers: The Moletta Tower Case Study

Original
Mitigation of Crowd-Induced Vibrations in Historic Masonry Towers: The Moletta Tower Case Study / Bali, A., Cardoni, A., Abderaouf Louar, M., Cimellaro, G.P.. - In: INTERNATIONAL JOURNAL OF ARCHITECTURAL HERITAGE. - ISSN 1558-3058. - (2026), pp. 1-20. [10.1080/15583058.2026.2683556]

Availability:
This version is available at: 11583/3017754 since: 2026-11-11T12:26:05Z

Publisher:
Taylor and Francis

Published
DOI:10.1080/15583058.2026.2683556

Terms of use:

This article is made available under terms and conditions as specified in the corresponding bibliographic description in the repository

Publisher copyright

(Article begins on next page)

21 November 2026



International Journal of Architectural Heritage
Conservation, Analysis, and Restoration

ISSN: 1558-3058 (Print) 1558-3066 (Online) Journal homepage: www.tandfonline.com/journals/uarc20

Mitigation of Crowd-Induced Vibrations in Historic Masonry Towers: The Moletta Tower Case Study

Adel Bali , Alessandro Cardoni , Mohamed Abderaouf Louar & Gian Paolo Cimellaro

To cite this article: Adel Bali , Alessandro Cardoni , Mohamed Abderaouf Louar & Gian Paolo Cimellaro (08 Jun 2026): Mitigation of Crowd-Induced Vibrations in Historic Masonry Towers: The Moletta Tower Case Study, International Journal of Architectural Heritage, DOI: 10.1080/15583058.2026.2683556

To link to this article: https://doi.org/10.1080/15583058.2026.2683556

© 2026 The Author(s). Published with license by Taylor & Francis Group, LLC.

Published online: 08 Jun 2026.

Submit your article to this journal

Article views: 479

View related articles

View Crossmark data

Full Terms & Conditions of access and use can be found at
https://www.tandfonline.com/action/journalInformation?journalCode=uarc20

INTERNATIONAL JOURNAL OF ARCHITECTURAL HERITAGE
https://doi.org/10.1080/15583058.2026.2683556

Taylor & Francis
by informa

RESEARCH ARTICLE

OPEN ACCESS Check for updates

Mitigation of Crowd-Induced Vibrations in Historic Masonry Towers: The Moletta Tower Case Study

Adel Bali[a], Alessandro Cardoni[a], Mohamed Abderaouf Louar[b], and Gian Paolo Cimellaro[a]

[a]Department of Geotechnical, Structural and Civil Engineering, Politecnico di Torino, Torino, Algeria; [b]Department of Mechanical Engineering, Ecole Militaire Polytechniques, Algiers, Algeria

ABSTRACT

Historic structures near large public gathering areas are increasingly exposed to dynamic loads from human activities, particularly during concerts and similar events. This study presents a numerical investigation of three mitigation strategies to protect the Moletta Tower from crowd-induced vibrations during large-scale events. A detailed finite element model of the Circus Maximus and the tower was developed to incorporate soil–structure interaction, realistic boundary conditions, and dynamic loading scenarios. The proposed strategies are: (1) installation of a Tuned Mass Damper Inerter (TMDI) within the tower to reduce structural vibrations; (2) deployment of a temporary foam-based vibration-damping mat to attenuate crowd-induced excitation at the source; and (3) implementation of subsoil barriers to dissipate ground-borne waves reaching the structure. Results indicate that the damping mat achieved the greatest reduction, lowering peak acceleration by up to 60%. Subsoil barriers provided variable performance, reducing vibrations by 15–45% depending on configuration, while the TMDI offered moderate attenuation, decreasing displacement by 10–40%. Each solution presents distinct advantages and limitations regarding feasibility, cost, and effectiveness. These findings provide valuable insights for safeguarding cultural heritage sites against anthropogenic dynamic loads.

ARTICLE HISTORY
Received 10 January 2026
Accepted 28 May 2026

KEYWORDS
Crowd dynamics; geofoam barrier; heritage preservation; human-induced vibrations; tuned mass damper

1. Introduction

The preservation of historical masonry structures located in densely populated urban areas is increasingly challenged by dynamic loads generated by modern public activities. Large-scale events such as concerts, festivals, and public celebrations introduce anthropogenic vibrations that were never considered in the original design of heritage buildings. This concern has been critically highlighted by recent structural failures, including the collapse of the medieval Torre dei Conti in Rome (Nadeau 0000), constructed between the 9th and 13th centuries, which has intensified awareness of the vulnerability of historic structures to contemporary loading conditions.

The activity of large crowds, particularly jumping and interacting in rhythm with music, can produce low-frequency ground vibrations, typically ranging from 1 Hz to 3.2 Hz (Bachmann and Ammann 1987). Although these vibrations are generally of limited amplitude, their repetitive, rhythmic, and lateral nature can significantly affect ancient masonry structures. Such buildings were not designed to withstand sustained dynamic excitation and often exhibit low tensile strength, limited damping capacity, and pronounced sensitivity to resonance phenomena. Human-induced loads are commonly classified according to the activity type, including walking (1–3 Hz), jumping (1.5–3 Hz), and dancing, which can generate vertical forces ranging from 0.5 to 3 times the body weight, characterized by either periodic or impulsive patterns.

Among these activities, jumping loads are recognized as the dominant source of dynamic excitation during large public events. Several analytical and experimental studies have proposed models to represent jumping actions under crowd loading conditions (J. Chen 2016; Nikooyan and Zadpoor 2011; Racic, Pavic, and Brownjohn 2009). While the contribution of a single individual is relatively small, the collective and synchronized movement of large crowds can produce measurable and sometimes critical ground vibrations (Bachmann 1995; Ellis and Ji 2004). Field measurements conducted during mass events have reported peak ground accelerations reaching values as high as 0.15 g in audience areas. Consequently, international standards such as ISO 10137 (International Organization For Standardization 2007) and UNI 9916 (UNI 2004)

CONTACT Gian Paolo Cimellaro gianpaolo.cimellaro@polito.it Department of Structural, Geotechnical and Building Engineering, Politecnico di Torino, Corso Duca degli Abruzzi 24, Torino 10129, Italy

© 2026 The Author(s). Published with license by Taylor & Francis Group, LLC.
This is an Open Access article distributed under the terms of the Creative Commons Attribution License (http://creativecommons.org/licenses/by/4.0/), which permits unrestricted use, distribution, and reproduction in any medium, provided the original work is properly cited. The terms on which this article has been published allow the posting of the Accepted Manuscript in a repository by the author(s) or with their consent.

provide serviceability criteria for vibration-sensitive structures, with particular emphasis on heritage buildings, where conservation requirements often restrict the application of conventional structural strengthening measures.

Given the vulnerability of the Moletta Tower to low-frequency ground vibrations generated during large-scale public events, there is a clear and urgent need for effective, non-invasive, and context-sensitive vibration mitigation strategies. These strategies are essential to ensure the long-term preservation of the tower while maintaining the urban functionality of the Circus Maximus as a public gathering space. One of the most extensively studied passive control systems is the Tuned Mass Damper (TMD), originally proposed by Frahm in 1909 (Frahm 1911). The TMD is a single degree of freedom system composed of a secondary mass attached to the main structure through a spring and a viscous damper. It is designed to reduce the amplitude of structural vibrations when tuned to the excitation frequency of the primary structure (Connor 2003; Zilletti, Elliott, and Rustighi 2012). To enhance its performance and reduce the required mass, an inerter was later integrated into the TMD system, forming what is now known as Tuned Mass Damper Inerter (TMDI). The inerter is a mechanical device that produces force proportional to the relative acceleration between two terminals. It can significantly increase energy dissipation efficiency while keeping the added mass to a minimum (R. Q. Chen et al. 2019; Garrido, Curadelli, and Ambrosini 2013; Mirza Hessabi and Mercan 2016). Several studies evaluated the performance of TMDI systems (De Angelis et al. 2019; Zilletti, Elliott, and Rustighi 2012) applied in slender, tall structures like wind turbines (Zhang et al. 2023) and towers (Bertollucci Colherinhas et al. 2019) to mitigate the combined seismic and wind dynamic loads. Therefore, TMDI could be a viable solution for historical towers with limited space and material strength to install a traditional TMD.

In addition to dynamic absorbers, polymer foam materials have gained attention as effective energy-dissipating layers for attenuating human-induced vibrations. Materials such as polyurethane (PU), rubber and ethylene vinyl acetate foam (EVA) possess excellent shock absorption properties, making them suitable for use in vibration isolation mats (Briody, Duignan, and Jerrams 2011; Gent 2005; Wu et al. 2023). Various behaviour models were introduced to define this material for finite element (FE) simulations. Among these, the Ogden-foam model (W. Li et al. 2023), which is the most recognized model that is used in different commercial FE software packages. Recent studies have quantified the strain-rate dependent behaviour of these materials under dynamic loading conditions (Kaewunruen et al. 2018). Their cellular structure allows for broadband attenuation of ground-transmitted energy, especially in the low-frequency range typical of crowd-induced excitation (1–3 Hz). These materials have been widely applied in packaging, sports surfaces, and impact safety systems (Altan 2018; N. Mills 2007).

Another promising mitigation strategy involves the implementation of subsurface vertical barriers to disrupt vibration transmission through the soil (Richart, Hall, and Woods 1970). Several studies including both field tests (Mahdavisefat, Salehzadeh, and Heshmati 2018; Massarsch 2005) and FE modelling (Coulier et al. 2015; Gao et al. 2018) have been carried out in order to evaluate the efficiency of the wave barrier. Originally studied by Woods (Woods 1968), open trench barriers were shown to reduce ground-borne vibrations by up to 75%. However, practical limitations such as soil instability and site constraints often make open trenches unfeasible. As an alternative, geofoam filled trenches have been investigated as passive vibration barriers. Field studies, such as those by Alzawi et al. (Alzawi and El Naggar 2011), demonstrated that geofoam-filled trenches can achieve up to 68% vibration attenuation, offering a more practical and sustainable solution to ensure the stability of the soil. Further research by Celebi et al. (Çelebi et al. 2009) described the results of experimental studies on the screening efficiency of open and stiff and soft materials filled trenches in the case of active and passive barriers. Vibration screening is classified into two categories including the active scheme, in which the obstacle is installed near the source of vibration, and the passive scheme, in which the trench is constructed far away from the vibration source. The observations illustrate that passive isolation is more effective than active isolation. Furthermore, softer back-fill material can be more effective in attenuating the incoming waves in comparison with stiff materials.

The main contribution of this research is the evaluation of vibration mitigation strategies specifically tailored to protect historic masonry structures subjected to human-induced dynamic loads during large-scale events. This study quantifies human-induced vibration effects in terms of structural response and investigates mitigation approaches aimed at reducing these demands through the implementation of technologies acting at different stages of the vibration transmission path. Furthermore, this study is motivated by the current lack of comprehensive analyses addressing the mitigation of human-induced vibrations in historic masonry structures during concert-type events. The analyses in this paper cover: (i) the integration of a TMDI within

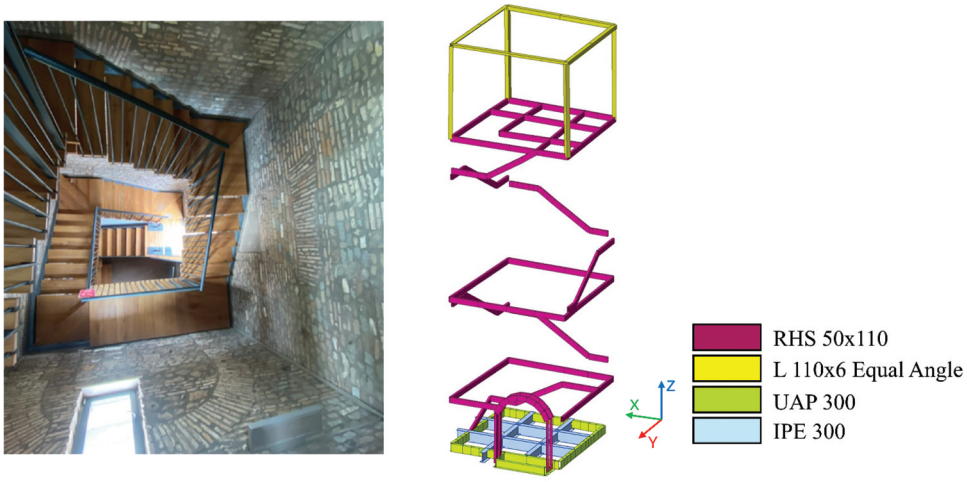


Figure 1. Steel beam stairs' shape: (a) real structure, (b) FE model.

the tower to reduce structural response, (ii) the deployment of a temporary foam-based vibration-damping mat to attenuate vibrations at the source, and (iii) the implementation of subsoil geofoam barriers to disrupt wave propagation before reaching the structure.

The primary objective of this study is to ensure the structural safety of the Moletta Tower while preserving its historical integrity within a dynamic urban environment. This objective is addressed by assessing the structural response at the top of the tower, with particular emphasis on vibration demands induced by concert-related excitations, which are adopted as the governing criterion for structural performance evaluation. The tower is frequently subjected to dynamic loads generated during large-scale public events such as concerts and festivals, events that have attracted up to 120,000 attendees (Puzzilli et al. 2021) during the 2004 World Cup victory celebration. By comparing the effectiveness, feasibility, and limitations of the proposed strategies, this study aims to identify viable solutions that align with the constraints and priorities of cultural heritage preservation.

2. Strategies proposed to mitigate the crowd-induced vibrations

2.1. Case study

The Moletta Tower, a medieval defensive structure constructed around 1145 and located in the Circus Maximus area of Rome, was selected as the case study for this research, features a squared plan with walls made of bricks and limestone. The tower exhibits non-uniform wall thicknesses, 0.9 m at the foundation level, 0.75 m at the ground level, 0.5 m at the middle level and 0.7 m at the top. The foundation level is located 4 m below the ground level. The tower occupies an area of 20 m^2. Its mechanical properties were cross-checked against the National Technical Code (NTC2018) (2018).

The masonry was modelled as an equivalent homogeneous material. The first three natural frequencies of the tower are 2.76 Hz, 3.05 Hz and 5.12 Hz, corresponding, respectively, to translational modes in the Y and X directions, followed by a torsional mode about the Z-axis. The natural frequencies and associated mode shapes were identified from in-situ acceleration records using the Frequency Domain Decomposition (FDD) method. The experimentally identified modal parameters were subsequently used in the calibration process. The close agreement between the numerical and experimental frequencies validates the use of an equivalent homogeneous material model to accurately represent the global dynamic behaviour of the structure.

The spiral staircase is supported by steel beams connected to the masonry walls. These beams consist of rectangular hollow sections (RHS), with a thickness of 3 mm and cross-sectional dimensions of 110 mm × 60 mm, as shown in Figure 1a. The structural frame of the top floor is composed of steel equal angle sections, with leg dimensions of 110 mm and a thickness of 6 mm. The base of the tower is reinforced with steel members, an I-beam 'IPE 300' and a U-beam 'UAP 300'. The geometry details of the steel element are shown in Figure 1b.

Table 1 summarizes the mechanical properties adopted for the masonry material after calibration, where the compressive strength (f_m) reflects the material

Table 1. Mechanical properties of the equivalent material.

f_m [MPa]	f_s [MPa]	f_t [MPa]	E [MPa]	G [MPa]	W [kN/m^3]	ν
3.26	0.07	0.38	1150	440	19	0.3

capacity to withstand axial loads, and the shear strength (f_s) and tensile strength (f_t) indicate relatively low resistance under shear and tension, respectively, as expected for typical masonry. The Young's modulus (E) represents the elastic stiffness under uniaxial stress, while the shear modulus (G) quantifies the material response to shear deformation. The unit weight (W) contributes to the structural self-weight and overall dynamic response and (ν) is the Poisson's ratio.

2.2. Tuned mass damper inerter model

This study adopts a linear model for the TMDI system implementation, which was placed at 10 m above the ground, at the same level of the top floor. It is supported by two IPE 180 steel beams parallel to the Y-direction (Figure 2a), which is the maximum beam height that can be reached respecting architectural and accessibility constraints. Placement on the roof was deemed unsuitable due to the light roof construction system composed of thin wooden beams and bricks, which lack the necessary load-bearing capacity.

Figure 2b shows the practical implementation, where the inerter terminals are connected using steel rods designed to ensure efficient force transmission and structural reliability. Terminal 1 is connected to the TMD mass through a steel rod made of S235, with a nominal diameter of 20–25 mm and attached via a bolted clevis joint using high-strength preloaded bolts (class 8.8) to ensure proper axial force transfer while allowing rotational flexibility and preventing unintended bending moments. Similarly, terminal 2 is connected to the foundation using a steel rod of same dimensions, which is anchored to a steel base plate (200 × 200 × 15 mm) fixed to the reinforced concrete foundation with four M20 anchor bolts (class 8.8) embedded to a sufficient depth to provide adequate pull-out and shear resistance. All connections are designed to ensure reliable load transfer, and all steel components are protected against corrosion through galvanization or appropriate protective coatings to ensure long-term durability.

2.2.1. Finite element modelling

Figure 2a represents the FE model of the tower equipped with TMDI. The masonry walls and the beams supporting the TMD were modelled using 3D solid elements, with element sizes of 0.25 m and 0.05 m, respectively. The steel stair beams were modelled as 1D elements with a length of 0.1 m. The complete FE model contained 8,250 nodes and 17,474 elements, resulting in 25,013 degrees of freedom.

The effect of placing the TMDI at the selected level was evaluated using linear static analysis, with particular attention to the load transfer from the supporting beams to the masonry walls. The goal was to assess the structural stability of the system consisting of the tower and supporting beams under

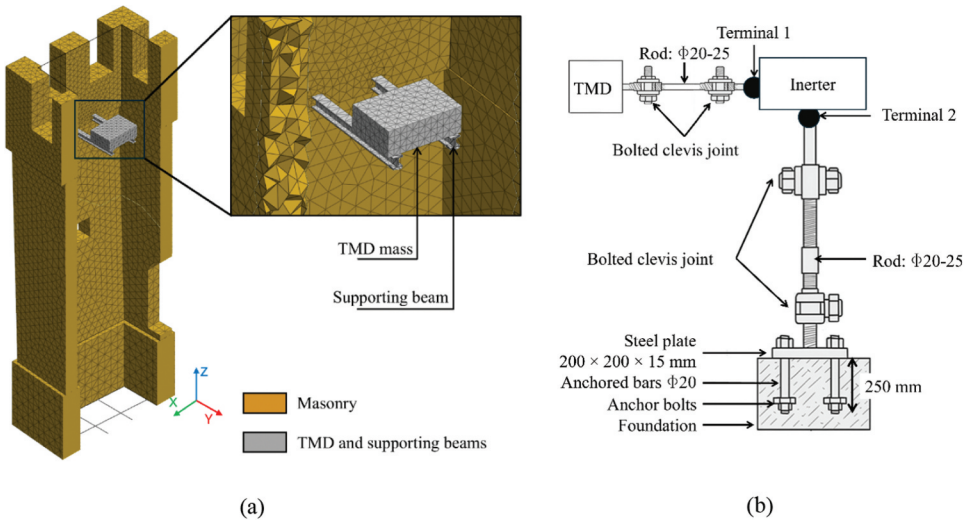


Figure 2. Tower equipped with TMDI: (a) FE model of the tower equipped with TMDI, and (b) schema of the connection between TMD, inerter, and foundation.

the additional static loading introduced by the TMDI. The results show a maximum compressive stress of 544 kPa in the masonry at the tower base and 1.76 MPa in the steel beams. These values remain well below the material limits, with the masonry compressive strength equal to 3.24 MPa according to NTC 2018 and the steel yield strength equal to 235 MPa according to Eurocode 3 (CEN 2005).

Modal analysis revealed a dominant first mode in the Y-direction with a frequency of 2.76 Hz, exciting over 59% of the modal mass, while higher modes contribute less than 8% each. The second mode has a frequency significantly higher (7.12 Hz). The identified modes exhibit clear spectral separation, and the structural response is governed primarily by the fundamental mode. These considerations led to modelling the MDOF tower as an equivalent SDOF system for the initial tuning of the TMDI. This simplification preserves the dominant dynamic characteristics of the structure in the direction of interest while significantly reducing computational complexity.

2.2.2. TMDI optimization with genetic algorithm

The inerter was configured in series between the TMD mass and the structure's base. This configuration was chosen to maximize the inertial amplification effect, where the device provides a large effective mass (inertance) with a small physical mass, which is crucial for the performance of the TMDI system. This simplification maintains the fundamental vibration characteristics while enabling computationally efficient parameter optimization, balancing accuracy with practicality for performance evaluation of the slender tower structure. The TMDI's non-dimensional parameters, i.e., the frequency ratio (f_t) and damping ratio (ζ_t), were optimized using a genetic algorithm (GA). The optimization objective was to minimize the peak amplitude of the frequency response function (FRF) of the fundamental SDOF system, as this directly correlates with reducing maximum displacement. The mass ratios (μ_t and μ_b) were treated as independent variables to explore their influence on the optimum f_t and ζ_t. The displacement response ($Y(\omega)$) is expressed in Equation 1. The optimization problem has a single objective, that is minimizing the peak FRF.

$$Y(\omega) = A(\omega)^{(-1)} f \tag{1}$$

In Equation 2, f is the dynamic load and $A(\omega)$ is the dynamic stiffness matrix of a given angular frequency ω.

$$A(\omega) = -\omega^2 M + i\omega C + K \tag{2}$$

The mass **M**, damping **C** and stiffness **K** matrices are shown in Equations 3, 4, and 5, respectively.

$$M = \begin{bmatrix} 1 & 0 \\ 0 & \mu_t + \mu_b \end{bmatrix} \tag{3}$$

$$C = \begin{bmatrix} 2\omega_s(\zeta_s + \zeta_t(\mu_t + \mu_b)f_t) & -2\omega_s\zeta_t(\mu_t + \mu_b)f_t \\ -2\omega_s\zeta_t(\mu_t + \mu_b)f_t & 2\omega_s\zeta_t(\mu_t + \mu_b)f_t \end{bmatrix} \tag{4}$$

$$K = \begin{bmatrix} \omega_s^2(1 + \mu_t f_t^2) & -\omega_s^2\mu_t f_t^2 \\ -\omega_s^2\mu_t f_t^2 & \omega_s^2\mu_t f_t^2 \end{bmatrix} \tag{5}$$

where: $\mu_t = \frac{m_t}{m_s}$ is TMD mass ratio, $\zeta_t = \frac{c_t}{2(\mu_t+\mu_b)\omega_t}$ is the damping ratio; *** is the frequency ratio; $\mu_b = \frac{m_b}{m_s}$ is the inerter mass ratio; m_s, *** and ζ_s are the SDOF mass, angular frequency and damping ratio of the superstructure; m_t, c_t and ω_t are the mass, damping and angular frequency of the TMD, while m_b is the effective mass of the inerter. The solution of Equation 1 is the amplitude of the FRF at the top of the tower ($|Y(1)|$).

The GA parameters were selected based on established literature values (Djerouni et al. 2021; Kim, Lee, and Lee 2024; Suryadi et al. 2023), as detailed in Table 2. It should be noted that μ_t and μ_b were excluded from optimization, as previous studies showed consistent convergence toward upper bounds (Djerouni et al. 2021; Kim, Lee, and Lee 2024; Suryadi et al. 2023). These parameters were instead treated as controlled variables, with μ_t systematically varied from 0.01 to 0.2 with an increment of 0.01, and μ_b, from 0 to 0.5 with increments of 0.02. This approach required reformulating the optimization problem to focus on mass ratio control, which directly influences the remaining system parameters. These parameters are constrained as follows: $\mu_t > 0$, $\mu_b > 0$.

The optimization results, illustrated in Figure 3, demonstrate the functional relationships between the TMDI system parameters and their mass ratios. Figure 3a illustrates the FRF magnitude, which exhibits an inverse correlation with both μ_t and μ_b, indicating better vibration attenuation for higher mass ratios. Figure 3b reveals that the optimum values of frequency

Table 2. GA parameters selected in the optimization process.

GA parameter	Value
Population size	200
Number of generations	100
Mutation probability	0.8
Crossover probability	0.015
Tolerance	1e-7

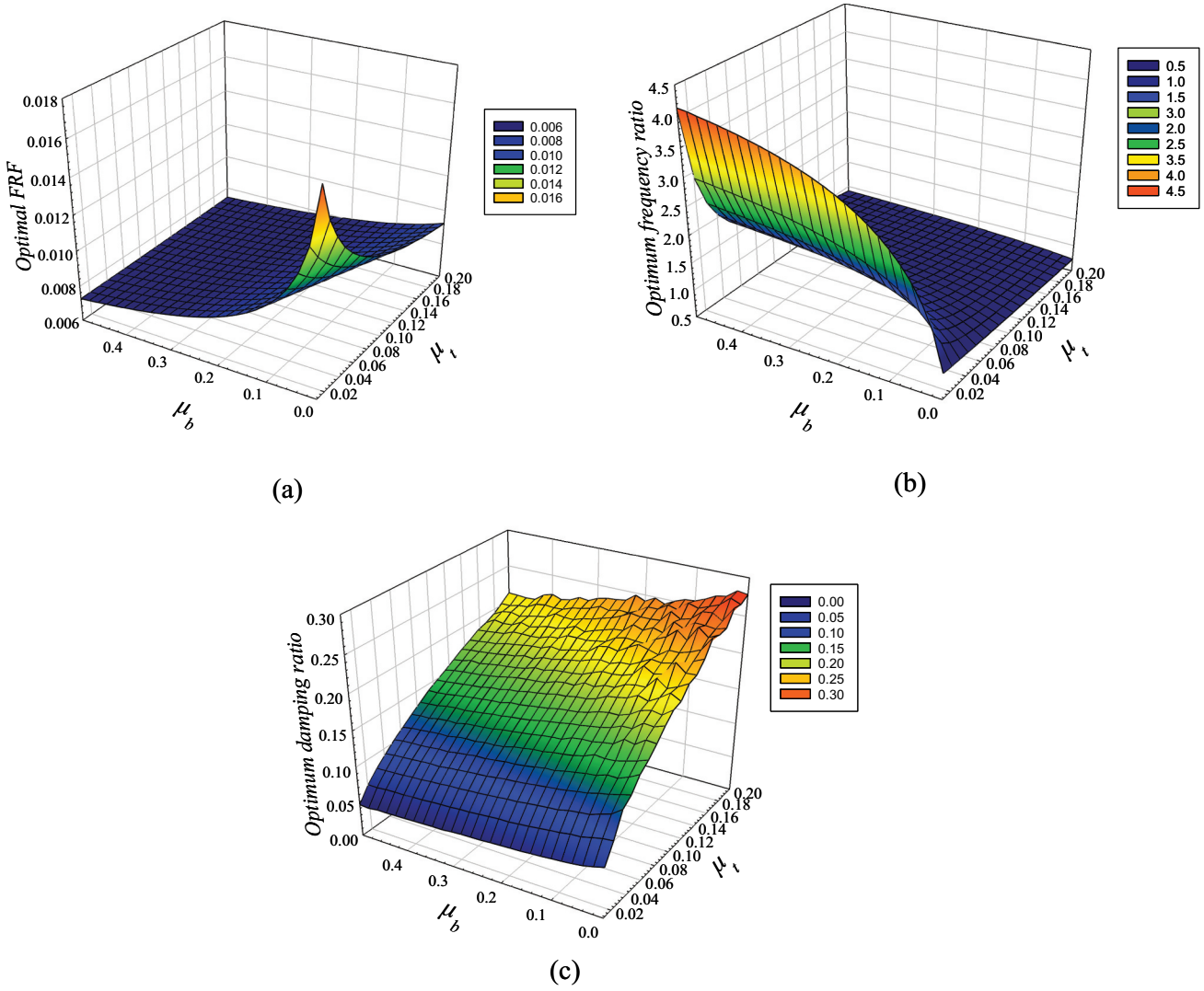


Figure 3. Results of optimization: (a) optimal values of FRF, (b) optimum frequency ratio and (c) optimum damping ratio function of TMD and inerter mass ratios.

ratio (f_t) display contrasting dependencies: it decreases with increasing μ_t but increases with μ_b, reflecting the distinct dynamic contributions of each component. Figure 3c shows a positive correlation between both mass ratios and the optimal damping ratio (ζ_t), suggesting enhanced energy dissipation requirements at higher mass configurations. These observed trends quantitatively demonstrate the coupled effects of mass distribution on the TMDI's frequency tuning and damping characteristics.

The selection of the TMDI mass ratios for the time-history analysis was done through an iterative optimization process that sought to balance performance with practical feasibility. The optimization revealed a strong correlation between higher mass ratios and improved vibration attenuation, as quantified by the reduction in the FRF peak. However, while the inerter provides a large effective mass with minimal physical mass addition, the TMD's physical mass directly contributes to the static load on the tower. The selected parameters are $\mu_t = 0.02$ and $\mu_b = 0.2$, which allow to achieve a significant 55% FRF reduction while keeping a low μ_t to mitigate static load concentration. The selected inerter ratio μ_b was set an order of magnitude higher to leverage its mass-amplification effect and maximize dynamic performance.

In cases where bidirectional vibration mitigation is required, the problem can be addressed using multi-degree-of-freedom TMD configurations, as reported in the literature (Tse, Kwok, and Tamura 2012; Yang, Sedaghati, and Esmailzadeh 2022). A practical and space-efficient solution consists of a single TMDI device with two orthogonal horizontal degrees of freedom. This configuration employs one mass block connected to two independent spring-damper-inerter systems aligned with the X- and Y-directions. The mass is thus

free to move in the horizontal plane, allowing simultaneous control of vibrations along both principal axes. The stiffness, damping, and inertance parameters can be independently optimized for each direction, enabling the system to target different natural frequencies and modal properties.

2.2.3. Time history analysis

The response of the building with and without TMDI is obtained by rewriting the known equation of motion into state space form. This is done by transforming the 2nd order differential equation into the 1st order state-space form as expressed in Equation 6:

$$\dot{Y}(t) = A \cdot Y(t) + B \cdot F(t) \tag{6}$$

where *Y(t)* is the state vector (Equation 7), which is composed of the displacement $y(t)$ and velocity $\dot{y}(t)$ vectors, **A** is the state matrix (Equation 8), **I** is the identity matrix, **B** is the input matrix (Equation 9), *F(t)* is the external load matrix (Equation 10), $\{\Lambda\}$ is the influence vector and $\ddot{u}_g(t)$ is the recorded accelerograms during different events.

$$Y(t) = \begin{bmatrix} y(t) \\ \dot{y}(t) \end{bmatrix} \tag{7}$$

$$A = \begin{bmatrix} 0 & I \\ -M^{-1}K & -M^{-1}C \end{bmatrix} \tag{8}$$

$$B = \begin{bmatrix} 0 \\ -M^{-1} \end{bmatrix} \tag{9}$$

$$F(t) = -[M]\{\Lambda\}\ddot{u}_g(t) \tag{10}$$

The optimal TMD's parameters, considered in this study, are shown in Table 3. It is important to clarify that the actual mass of the inerter corresponds to its material weight, whereas its inertance represents the equivalent dynamic mass it imparts to the system through its internal mechanism.

To quantify the impact of human-induced vibrations on the structural response of the tower, the accelerations were recorded using a triaxial accelerometer installed at the tower's base during four major concert events: July 9, 2022; May 1, 2024; September 27, 2024; January 1, 2025. The PGA recorded in each event was, respectively, 1.92 cm/s^2, 1.02 cm/s^2, 1.96 cm/s^2 and 5.42 cm/s^2. In the analysis, only the time windows with large excitations were considered (Figure 4).

Figure 5 demonstrates the control system's effectiveness for each event through time history analysis, showing a 10% to 45% reduction in displacement amplitudes when the passive control system is implemented.

2.3. Foam-based vibration-damping mat

To evaluate the effectiveness of the foam mat placed on the soil surface, two loading scenarios were considered. In the first scenario, the loading generated by a person jumping directly on the bare soil is considered, hence, simulating direct contact. In the second scenario, the jumping load is applied on a 5 cm thick foam mat, creating an indirect contact condition which aims to reduce transmitted vibrations. The 5 cm thickness was selected as a representative compromise between vibration attenuation performance and practical mat flexibility for sport event deployment (Tomin and Kmetty 2022).

Table 3. Physical and non-dimensional optimal TMD's parameters.

TMD mass ratio	Inerter mass ratio	Frequency ratio	Damping ratio	TMD's actual mass [ton]	Inerter effective mass [ton]	Inerter actual mass [kg]	Damping [kN. s/m]	Stiffness [kN/m]
0.02	0.2	1.2	0.1	1.77	17.7	170–250	97.2	880

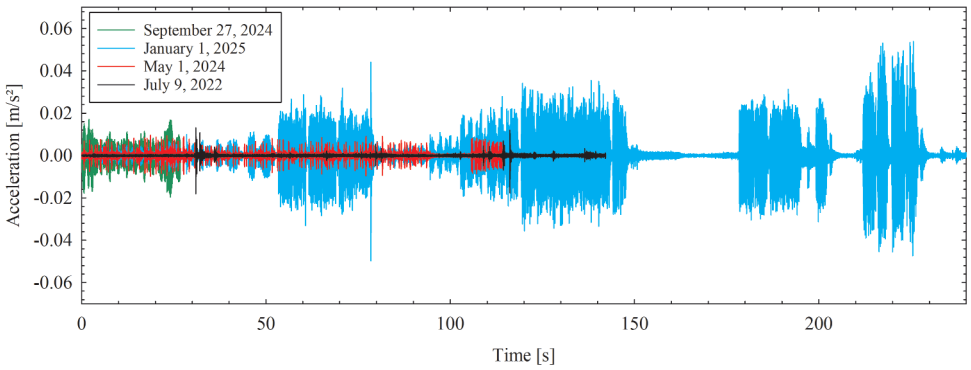


Figure 4. Base excitation input: recorded peak accelerations at the base of the tower.

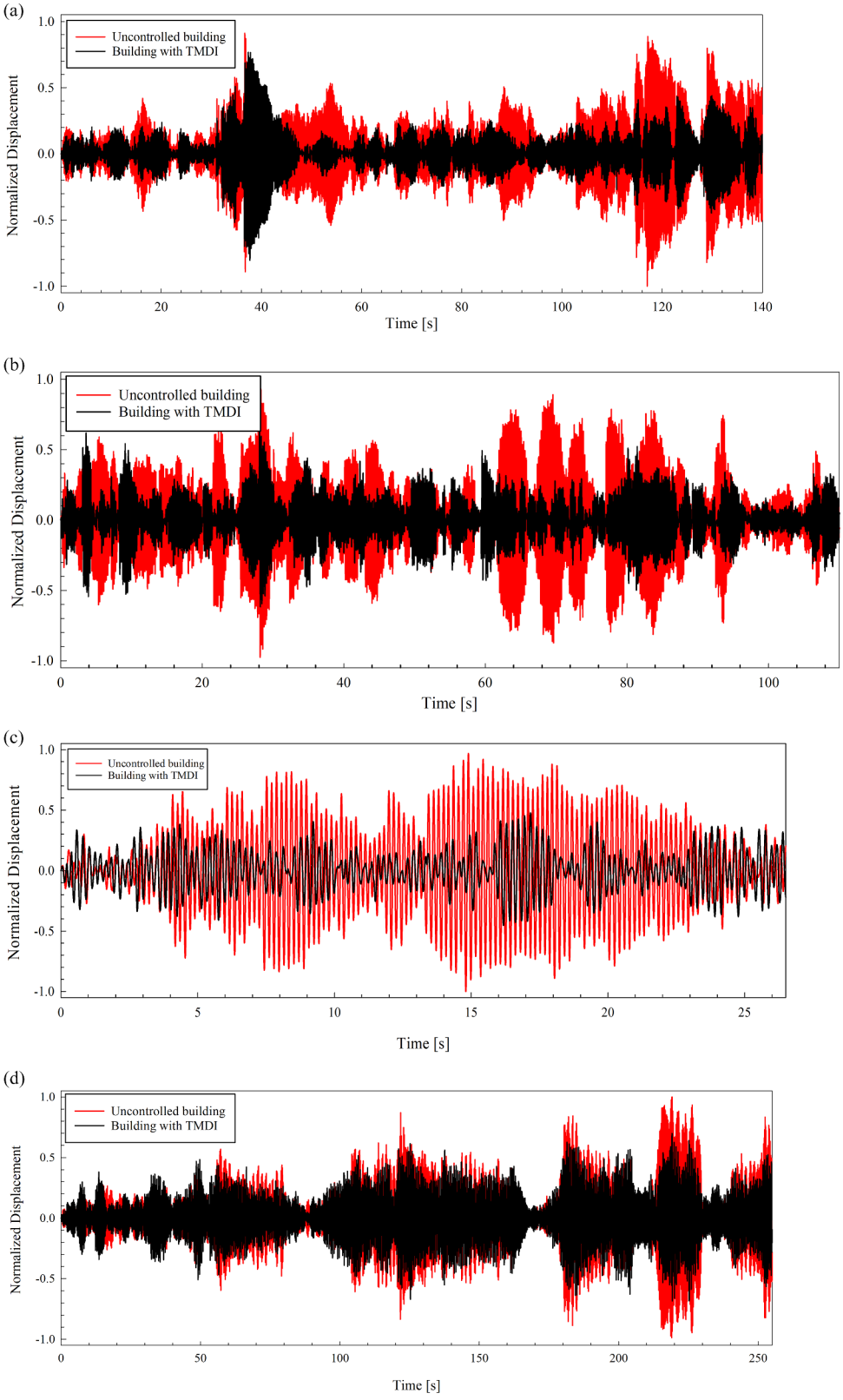


Figure 5. Normalized structural displacement of the tower equipped with TMDI, relatively to the uncontrolled building, under crowd-induced vibrations at: (a) July 9, 2022, (b) May 1, 2024, (c) September 27, 2024, and (d) January 1, 2025.

Three foam materials were selected for the vibration-damping mat solution: PU, EVA, and rubber foam. Both monolayer and multilayer arrangements were proposed to investigate their performance.

2.3.1. Loading modelling

The development of reliable models for jumping-induced loads has often involved simulating vertical force time-history functions. Among the pioneering investigations, Bachmann and Ammann (Bachmann and Ammann 1987) (1987) proposed that a series of identical half-sine wave pulses provides an effective representation of measured jumping force pulses. Later, various studies adopted this model to assess human activity effects on buildings such as (Fernández Martínez et al. 2016; Z. Li, Zhang, and Fan 2022; Sim et al. 2008). This model (Equation 11) was adopted to simulate the dynamic jumping action.

$$\begin{cases} F_s = K_p \cdot G \cdot \sin\left(\frac{\pi}{t_p} \cdot t\right) & 0 \le t \le t_p \\ F_s = 0 & t_p \le t \le T_p \end{cases} \quad (11)$$

In Equation 11, K_p represents the dynamic impact factor, F_s denotes the dynamic load, and G is the individual's weight. The temporal characteristics are described by contact duration (t_p) and pace period (T_p) calculated as the inverse of the stepping frequency (f_s), and the contact ratio is defined as t_p/T_p. The simulation considered a person weighing 800 N jumping at a frequency of 2 Hz for a duration of 3 min. Based on a contact ratio of 0.4, a dynamic impact factor K_p of 2.8 was adopted from established correlations in the literature (Bachmann 1995; Jones, Reynolds, and Pavic 2011). The person's weight is divided equally between both feet and applied on a footprint area of 0.04 m^2 as shown in Figure 6a. This load is treated as a uniformly distributed dynamic load with a peak value of 28 kN/m^2.

2.3.2. Finite element modelling

The FE model considered in this study is a specimen corresponding to the space occupied by a single person, with an area of $0.5 \times 0.5\ m^2$ and a depth of 1 m. This depth is significantly larger than the wavelength of the induced vibrations, so that it is possible to exclude the influence of wave reflections from the model's lower boundary on the foam–soil interface.

The model integrates both hyper-elastic and viscoelastic behaviours for the foam material. Furthermore, the soil was modelled as linear elastic, an assumption justified by the low-strain, elastic nature of wave propagation under small vibrational loads. A rigid simplified footprint was introduced at the top of the mat to reproduce load transfer from the person to the underlying foam layer. The footprint, mat, and soil are all modelled using 3D solid tetrahedral elements. The mesh sizes are defined as follows: 0.5–2 cm for the footprint, 1–3 cm for the mat, and 5–10 cm for the soil domain. The FE model was based on the testing apparatus originally used by White et al. (White 1998). Figure 6 illustrates the FE models developed to evaluate the performance of the foam mat in mitigating ground transmitted vibrations. Figure 6a depicts the direct contact scenario, where the individual is in contact with the soil without any isolation layer. In contrast, Figure 6(a, b) show the isolated soil configurations, where the individual jumps on a foam vibration-damping mat placed above the soil. The isolated configurations comprise two primary designs: a homogeneous monolayer system (Figure 6b) and a multilayered one (Figure 6c). The composite configuration is characterized by a 1 cm surface layer of high-density rubber for load redistribution, combined with a 4 cm substrate of compliant foam (PU or EVA) for enhanced energy dissipation.

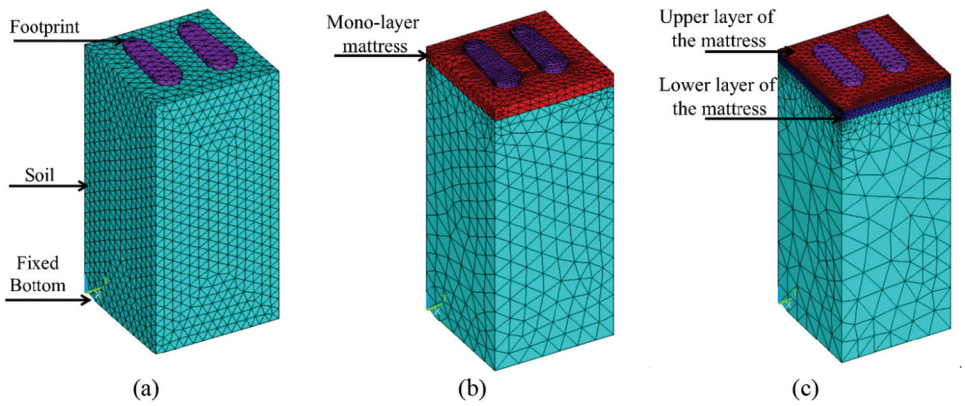


Figure 6. FE analysis of vibration transmission in soil systems under jumping loads: (a) non-isolated soil, (b) monolayer mat isolation, (c) multilayer mat isolation.

2.3.2.1. Hyper-elastic behaviour. The stress–strain behaviour of polymer foam is modelled in Ansys using the Ogden model (Khaniki et al. 2022) which is well suited for simulating the near-complete compressibility of foams by coupling volumetric and deviatoric responses to its strain energy density function (W). The formulation of the latter is expressed in Equation 12 (Brown et al. 2009):

$$W = \sum_{i=1}^{N} \frac{2\mu_i}{\alpha_i^2}\left(\lambda_1^{\alpha_i} + \lambda_2^{\alpha_i} + \lambda_3^{\alpha_i} - 3\right) + \sum_{i=1}^{N} D_i (J-1)^{2i} \tag{12}$$

where μ_i, α_i, and D_i are material-specific parameters determined experimentally, J is the elastic volume ratio, λ_i are the principal stretches, and N is the model order.

A third-order model ($N = 3$) was selected for this study as it provides a good balance between model complexity and accuracy in capturing the large-strain compression behaviour of foams across the expected strain range. Under uniaxial compression, the transverse stretches can be considered negligible for foams, which typically have a Poisson's ratio (ν) close to zero (W. Li et al. 2023). This allows to simplify the 3D formulation to a monodirectional uniaxial compression stress (σ_c) as a function of the axial stretch (λ), leading to the simplified expression in Equation 13.

$$\begin{aligned}\sigma_c &= \frac{\partial W}{\partial \lambda_1} \\ &= \sum_{i=1}^{N} \frac{2\mu_i}{\alpha_i}\left(\lambda_1^{\alpha_i - 1} - 2\nu\lambda_1^{-\alpha_i \nu - 1}\right) + 2(1-2\nu)\lambda_1^{-2\nu} \\ &\quad \times \sum_{i=1}^{n} i D_i (J-1)^{2i-1}\end{aligned} \tag{13}$$

The model parameters (μ_i, α_i, D_i for i = 1,2,3) were calibrated against the experimental stress–strain curves of PU (W. Li et al. 2023), EVA (Wu et al. 2023) and rubber (Guo et al. 2015), with densities of 25, 35, and 45, respectively, by optimizing the fit to Equation 13. This optimization was performed using a GA to minimize the error between the model prediction and the experimental data. The GA parameters used for this calibration are summarized in Table 4.

The goodness of fit R^2 is equal to 0.99, indicating an excellent fit between the fitted curve and the experimental values of PU (see Figure 7). The optimal values of the variables (μ_i, α_i, D_i) are shown in Table 5.

Table 4. Parameters of GA for optimization process.

Parameters	Value
Population size	200
Number of generations	800
Mutation probability	0.5
Crossover probability	0.8
Tolerance	1e-8

2.3.3. Prony series for viscoelastic behaviour

Under dynamic loading, the foam materials exhibit viscoelastic behaviour, meaning their mechanical response is strain rate dependent. Considering this latter is critical for accurately modelling energy dissipation under impact-like loads such as jumping.

This viscoelastic behaviour was modelled using a Prony series expansion within a generalized Maxwell framework (N. J. Mills 2006; Tapia Romero, Dehonor Gomez, and Lugo Uribe 2020). This model consists of several Maxwell elements (a spring and a dashpot in

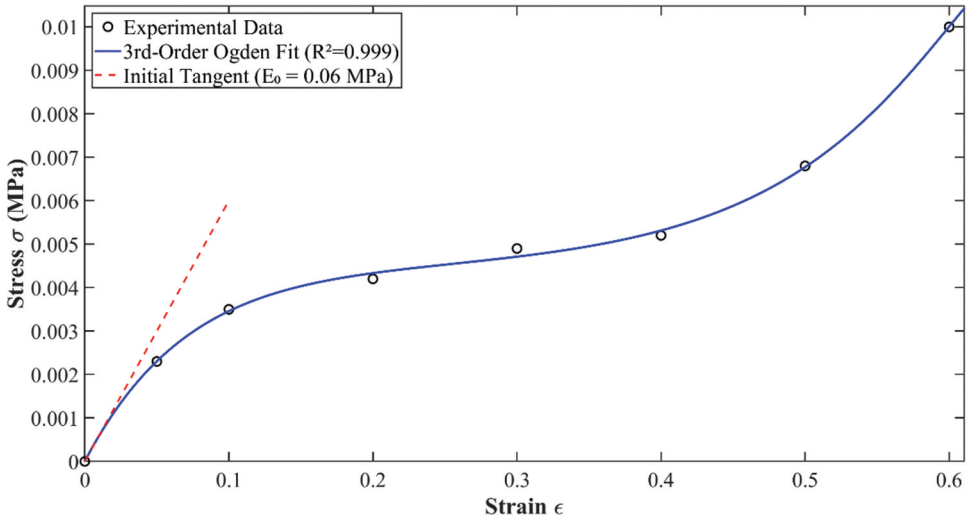


Figure 7. Fit between experimental data and optimized curve.

Table 5. Optimal values of the hyper-elastic model.

Material	Term	μ [MPa]	α	*D*
PU	1	0.2688	16.9948	−0.0034
	2	0.0023	1.3955	0.0044
	3	−0.3014	17.2031	−0.0159
EVA	1	−0.0808	8.0480	−0.5561
	2	0.0239	1.6019	0.8569
	3	0.0027	1.6101	−1.3171
Rubber Foam	1	1.1214	13.4205	−1.9963
	2	−3.7467	13.1773	−0.9899
	3	1.1750	6.5175	−3.0364

series) connected in parallel, plus an additional elastic spring to represent the long-term equilibrium stiffness. The Prony series formulation defines the time-dependent relaxation of the shear modulus, G(t) and is implemented in most FE software packages using the expression in Equation 14:

$$G(t) = G_0\left(1 - \sum_{i=1}^{n} g_i \exp(-t/\tau_i)\right) \tag{14}$$

where G_0 is the instantaneous shear modulus, g_i are dimensionless shear relaxation coefficients, and τ_i are the corresponding relaxation times. The sum of the relaxation coefficients must be less than one ($\Sigma g_i < 1$) to ensure that the long-term equilibrium modulus, $G_\infty = G_0(1 - \Sigma g_i)$, remains positive.

The instantaneous shear modulus G_0 was derived from the initial hyper-elastic Young's modulus E_0 and the assumed Poisson's ratio ($\nu \approx 0$) using the relation expressed in Equation 15.

$$G_0 = \frac{E_0}{2(1+\nu_0)} \tag{15}$$

The material properties of PU, EVA, and rubber were derived from experimentally validated literature sources (Guo et al. 2015; Sadeghnejad et al. 2019; Zhu and Mills 1999). For PU foam, the normalized shear moduli based on the work of Zhu and Mills (Zhu and Mills 1999) who characterized solid PU through stress relaxation tests were adopted. The EVA was modelled using a viscous formulation with parameters $g_1 = 0.195$ and $\tau_1 = 0.91$, as established by Sadeghnejad et al. (Sadeghnejad et al. 2019). For rubber, a generalized Maxwell model with coefficients $g_i = [0.5, 0.3, 0.1]$ and relaxation times $\tau_i = [0.1, 1, 10]$ from reference (Guo et al. 2015), was implemented.

2.3.4. Vibration attenuation performance of foam mats

The performance of the different vibration-damping mat configurations is summarized in Figure 8, which compares the reduction in peak surface acceleration relative to the non-isolated soil case. Single-layer mats exhibited distinct performance levels: PU foam achieved a 22% reduction, EVA foam a 50% reduction and rubber foam provided the highest reduction at 60%. The multi-layer configurations did not show a synergetic effect but rather a performance in between one of their constituent layers. The rubber–PU combination achieved a 40% reduction, and the rubber–EVA combination achieved a 55% reduction. In the combination design, the rubber

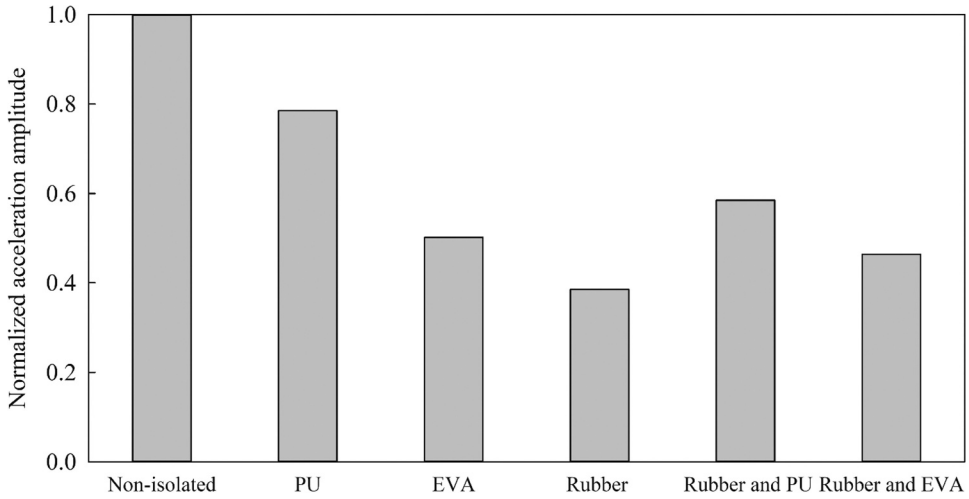


Figure 8. Normalized soil acceleration amplitudes under harmonic loading.

layer was placed at the surface to maximize its efficiency in redistributing the impact load and reducing stress concentrations, while the EVA layer underneath provided a compliant, lightweight support.

Although pure rubber foam showed the best performance, its high density makes it less practical for large-scale temporary events due to weight and handling constraints. The rubber-EVA configuration balances effective vibration mitigation (55% reduction) with practical weight constraints. Therefore, based on this trade-off between performance and practicality, the rubber–EVA combination is identified as the most viable solution for the intended application of protecting archaeological sites during temporary concerts.

Following the experimental assessment of vibration attenuation at the soil surface, the measured reduction in human-induced vibration loads (approximately 55%) was incorporated into the numerical model shown in section 2.4 to simulate the installation of the rubber–EVA mat system. Figure 9(a, b) present the FE simulation results of the acceleration time-history responses at the base and top of the tower, respectively. The results indicate a consistent reduction in structural response, with the tower acceleration decreasing by approximately 53.1% at the base and 54.8% at the top. These results demonstrate that the proposed mitigation strategy effectively reduces the dynamic response of the structure and confirms the potential of lightweight vibration isolation mats as a practical protective measure for heritage structures exposed to crowd-induced vibrations.

2.4. Subsoil geo-foam barriers

This section evaluates the effectiveness of passive wave barriers, a mitigation strategy that reduces vibration transmission through the soil before it reaches the structure. The specific solution investigated is a vertical trench barrier filled with geofoam, a lightweight, cellular geosynthetic material. These barriers function by creating a stark impedance contrast with the native soil, causing incident waves to be scattered and absorbed, thereby forming a protective (shadow) zone behind the barrier. A 3D finite element model of the Circus Maximus, including the Moletta Tower and the proposed wave barriers, was developed in the MIDAS FEA NX software (Figure 10). It extends over a total

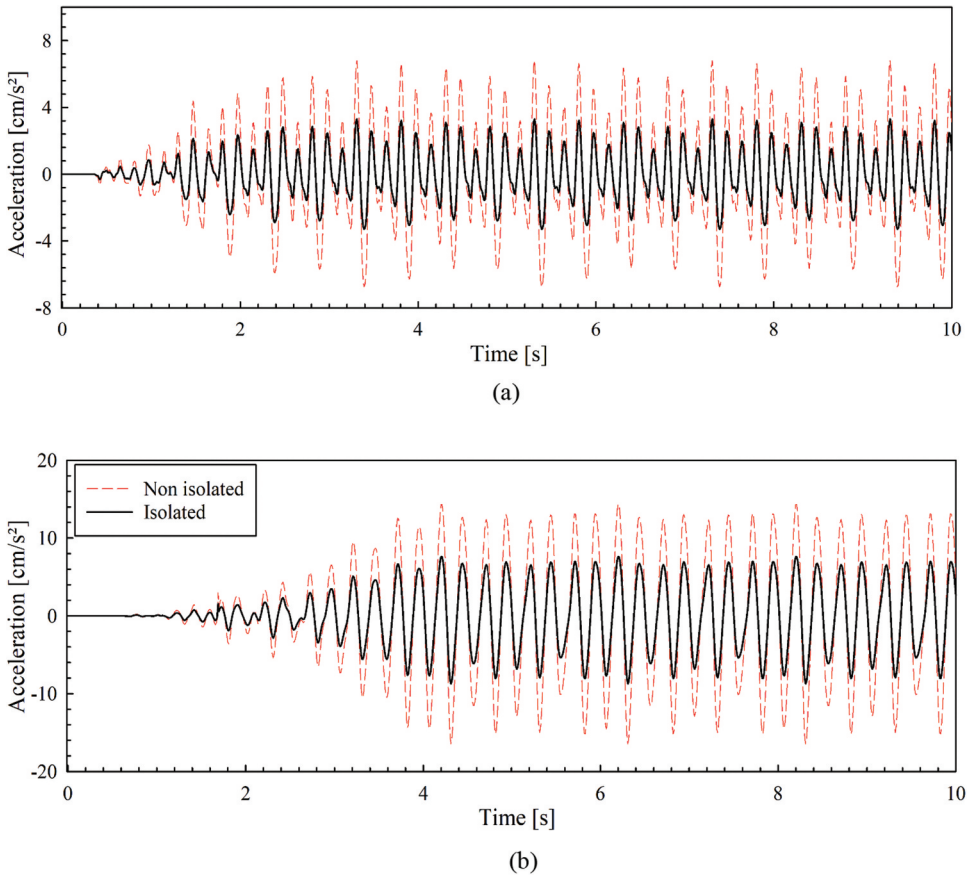


Figure 9. Time history analysis before and after adding rubber-EVA vibration-damping mat at: (a) the base and (b) the top of the tower.

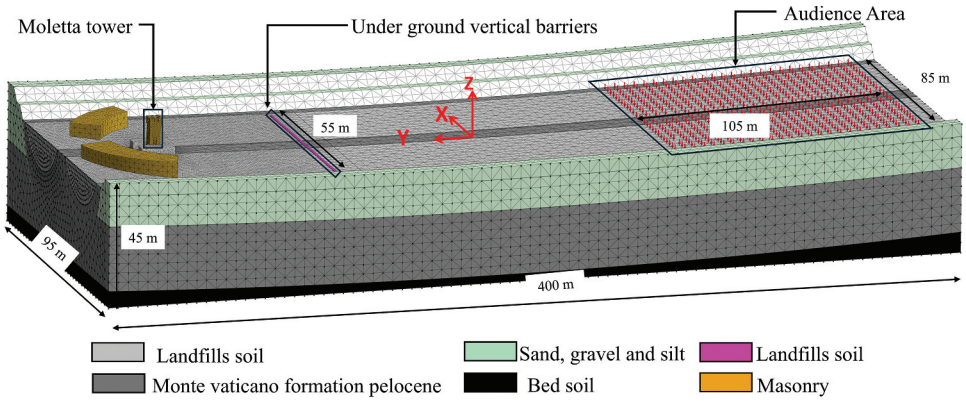


Figure 10. 3D FE model of Circus Maximus including Moletta tower and geo-foam barrier.

plan dimension of 400 m in length and 95 m in width, with a depth of 45 m to adequately capture wave propagation effects within the soil medium. The underground barriers extend longitudinally for 55 m and are positioned between the vibration source and the protected area. The audience area is defined by plan dimensions of 105 m × 85 m. The stratigraphy was based on the geological study carried out by Carpentieri et al. (Carpentieri, De Rita, and Monica 2015). The soil layers were modelled using 8-noded and 4-noded solid elements. A linear elastic constitutive model was adopted for all soil layers. This simplification is justified for this serviceability-level analysis, as the focus is on low-strain wave propagation under vibrational loads, a primarily elastic phenomenon. Historical records confirming no prior soil damage during large entertainment events further support this assumption. Lateral boundary conditions are modelled using infinite elements to simulate a continuous semi-infinite medium, thereby minimizing wave reflection artifacts at the model boundaries. This approach, aligned with the methodology of Su and Wang (Su and Wang 2013), is effective to avoid the boundary conditions' effects. A mesh convergence study was conducted to ensure that results were element size independent. The final mesh characteristics are summarized in Table 6.

To evaluate the effectiveness of the barriers in mitigating vibrations from a synchronized crowd, a nonlinear time-history analysis was performed. The dynamic load was simulated using the half-sinusoidal model described in section 2.3. Following ISO 10137 (International Organization For Standardization 2007), a crowd density of 3 people/m^2 was considered. This density corresponds to a dense crowd scenario, representing a conservative loading condition for the analysis. For an estimated attendance of 30,000 people, this resulted in a loaded area of approximately 10,000 m^2. The simulation modelled the entire crowd jumping simultaneously for a duration of 3 min. The resulting uniform pressure was applied over the designated audience area, and the propagation of the induced vibrations through the soil domain was simulated.

The geotechnical properties for the different soil layers, presented in Table 7, were sourced from site-specific investigations (Brancaleoni et al. 2015; Carpentieri, De Rita, and Monica 2015; Moscatelli et al. 2014). The unit weight (ρ) indicates the weight of soil per unit volume. The cohesion (C) represents the soil's shear strength component independent of friction. The internal friction angle (Φ) reflects the soil's resistance to shearing along internal planes. V_p and V_s denote the primary (compressive) and secondary

Table 6. Key features of the non-isolated FE model.

Nodes	Elements	Degrees of freedom	Number of equations	Circus soil mesh size [m]	Masonry walls mesh size [m]
52,229	274,856	178,176	168,138	4	0.35

Table 7. Mechanical properties of stratified Circus Maximus soil.

Soil	ρ[KN/m^3]	C [kPa]	Φ [°]	V_p [m/s]	V_s [m/s]	E [MPa]	G [MPa]	v
Landfill consists of various mortar and concrete	18	0–10	27–30	1300 ± 336	529 ± 148	966.3–302.1	341.6–106.2	0.42
Holocene alluvial sediments	20	0	40	2002 ± 398	582 ± 158	991.3–385	372.1–131.3	0.458
Volcanic sediment (bed soil)	20.5	76	24	1791 ± 337	473 ± 81	671.8–338	229.1–115.4	0.467
Sand gravel and silt	20	0	40	1078	390	344.02	119.9	0.435
Monti Vaticano	20.5	76	24	1791 ± 337	473 ± 81	671.8–338	229.1–115.4	0.467

(shear) wave velocities, respectively. They are used to evaluate dynamic soil behaviour. The Young's modulus (E) and shear modulus (G) quantify the soil stiffness under axial and shear loading. Lastly, Poisson's ratio (ν) describes the ratio of lateral to axial strain under loading. These parameters provide a comprehensive characterization of the soil mechanical and seismic response properties essential for structural and site response analyses.

A parametric study was conducted to systematically evaluate vibration barrier effectiveness in reducing ground-borne accelerations by examining both geometric and material properties. The investigation focused on three critical design parameters: distance between the geo-foam barrier and the tower, Young's modulus of the barrier material (0.05–500 MPa), installation depth (5–15 m), barrier thickness (0.5–2 m) and the shadow zone. The acceleration propagation was monitored in several points, starting from 5 m before the barrier (upstream, towards the audience area) to 30 m after the barrier (downstream, towards the tower). This multi-variable approach enabled rigorous comparison of 60 barrier configurations in addition to the non-isolated model as reference, with particular attention to their wave scattering and impedance matching capabilities.

2.4.1. Effect of the distance between geofoam barrier and the tower

The positioning of the geofoam barrier relative to the Moletta Tower was investigated as a critical design parameter influencing its effectiveness. The performance was measured by the reduction in peak acceleration at the tower base, normalized against the peak acceleration in the original configuration without barrier. The results, presented in Figure 11, demonstrate the attenuation efficiency for a barrier with a fixed geometry (thickness = 1 m, depth = 15 m) and Young's modulus (E = 1 MPa). The analysis showed that barriers located close to the tower are more effective, especially in the first 20 m. However, due to practical site constraints and the presence of underground ruins, the closest the barriers could be placed is at 30 m from the tower.

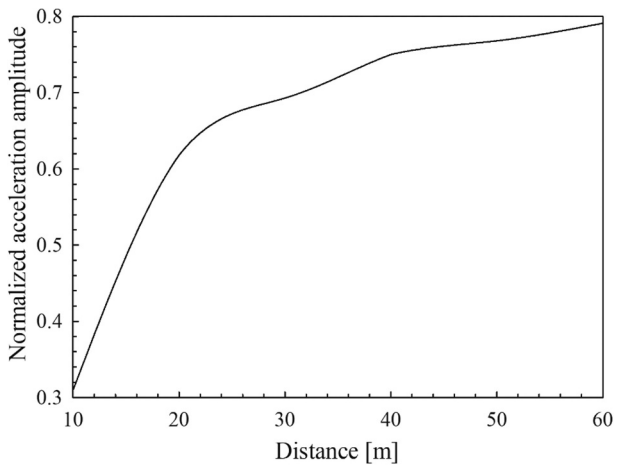


Figure 11. Acceleration attenuation varying the distance between the barriers and the tower.

2.4.2. Effect of stiffness of the geofoam barrier

The small strain levels developed in the geofoam material justified the assumption of linear elastic behaviours, with Young's modulus values considered in the range of 0.05 MPa to 500 MPa, consistent with the mechanical properties of commercially available geofoam products. The influence of the geofoam Young's modulus on vibration attenuation is presented using a logarithmic horizontal scale, as shown in Figure 12a. Figure 12b highlights the region corresponding to lower values of Young's modulus in order to ensure clearer visualization and interpretation within the broad stiffness range investigated. The results indicate that decreasing the Young's modulus, corresponding to increased geofoam flexibility, leads to a significant improvement in vibration attenuation efficiency. This behaviour is attributed to the enhanced impedance contrast between the soil and the geofoam barrier, which promotes reflection and attenuation of propagating vibration waves, thereby reducing the transmitted vibration energy toward the protected structure.

While an open trench (unfilled) configuration provides the best isolation performance, soil stability considerations require trench filling to mitigate stress concentration that could lead to ground instability effects.

2.4.3. Effects of the geofoam's thickness

Figure 13 shows the FE simulation results of the accelerations at the tower base for 1 MPa stiffness barriers, comparing three thicknesses (0.5 m, 1 m and 2 m) and depths (5 m, 10 m, and 15 m). The results demonstrate that vibration reduction improves with increasing barrier thickness. Each thickness increment between 0.5 m and 2 m provides about 5% additional acceleration reduction at the tower base. While deeper barriers consistently perform better and have a more beneficial effect, the 5% vibration reduction related to thickness increments remains across all depths.

2.4.4. Effect of depth of the geofoam barrier

This sensitivity analysis examined the effect of three different trench depths 5 m, 10 m and 15 m. As shown in Figure 14, geofoam trenches with a constant

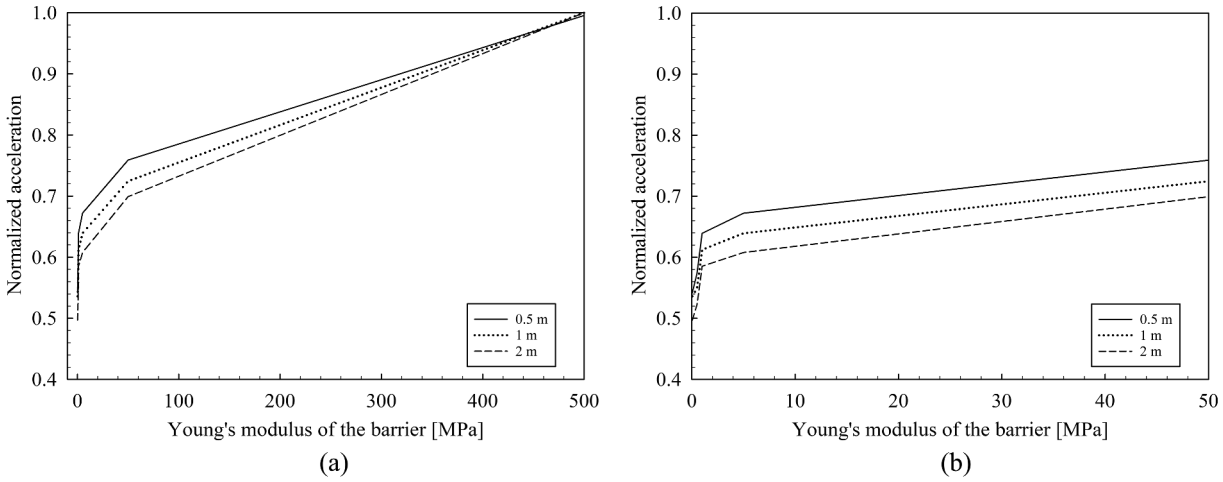


Figure 12. Barriers' stiffness effect on the acceleration reduction relative to the non-isolated model.

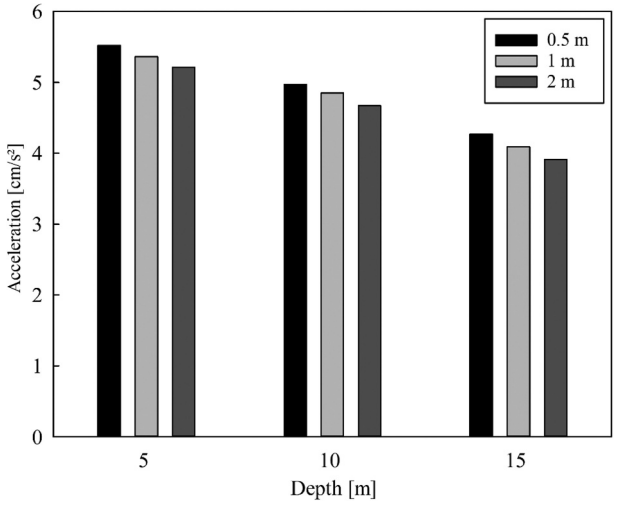


Figure 13. Barrier's thickness and depth effect on the acceleration at the base of the tower.

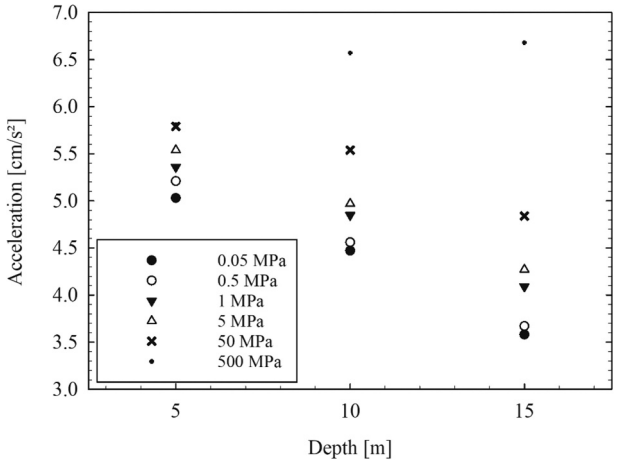


Figure 14. Barriers' depth effect on the acceleration.

thickness of 1 m were tested while varying material stiffness. The results demonstrate that trench depth significantly impacts vibration isolation performance. The shallowest trench proved to be the least effective, while the deepest configuration provided the greatest reduction in vibration acceleration at the tower base, except when using stiffer barrier materials.

2.4.5. Shadow zone effect

Figure 15 presents the measured acceleration results for points positioned both upstream (negative Y-axis values) and downstream (positive Y-axis values) of the geofoam barrier. The analysis revealed a significant reduction in vibration amplitudes directly behind the barrier (nearest monitoring point), demonstrating its effectiveness in wave attenuation. After a certain distance, acceleration levels start increasing as vibrations propagate from underneath the barriers. Then, vibra-

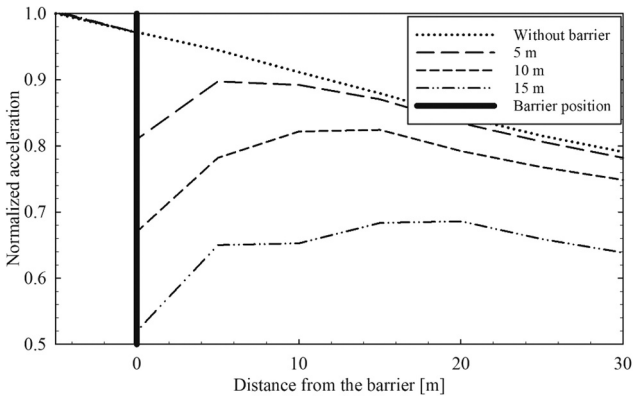


Figure 15. Spatial decay of acceleration amplitudes normalized to the peak upstream value.

tions decay again due to damping and wave dispersion effects.

3. Discussion

The results of this study showed that each vibration mitigation strategy presents distinct advantages and limitations when evaluated across criteria such as vibration reduction performance, material durability, implementation complexity, cost-
and limitations when evaluated across criteria such as vibration reduction performance, material durability, implementation complexity, cost-effectiveness, impact on cultural heritage sites, operational constraints. The next subsections discuss these points, highlighting the main trade-offs that must be considered for practical applications.

3.1. Vibration reduction performance

The foam-based vibration-damping mat emerged as the most effective solution, achieving up to 60% reduction in peak accelerations when using pure rubber foam. The EVA-rubber configuration maintained strong performance (55% reduction) considering the much lighter weight and consequent easier installation. Subsoil geofoam barriers showed variable effectiveness (15–45% reduction), with performance highly dependent on barrier depth and stiffness. It is worth mentioning that, in case the foam mats absorb water, their impact absorption capacity is significantly compromised. This reduces the compressibility and elasticity of the foam, limiting its ability to dampen energy effectively. Consequently, it leads to a stiffer response, higher peak forces transmitted to the protected structure, and a faster degradation of the material. The TMDI system provided moderate vibration attenuation (5–40%), with its effectiveness being particularly sensitive to proper tuning for the structure's modal characteristics and the input excitations.

3.2. Material properties and degradation

Each mitigation strategy differs not only in effectiveness but also in expected service life and maintenance requirements. Passive tuned mass damper systems are designed for long-term use, with main components engineered for ≥50 years of service, though damper elements may require replacement after roughly 10–15 years and inspections every 1–2 years to ensure performance (Matta 2021; TMD). Foam-based vibration-damping mats, while relatively simple and low-cost, are more susceptible to environmental degradation due to moisture, freeze–thaw effects, and mechanical wear, suggesting shorter service lives on the order of a decade in adverse conditions and replacement after performance loss (Zhou and Su 2023). Subsoil geofoam barriers, which are buried and protected from surface wear, may remain effective for approximately 10 years before potential replacement is needed in response to flooding or significant soil movements (Kaewunruen and Martin 2018). These differences in lifecycle and maintenance effort should be considered alongside effectiveness when evaluating mitigation strategies for heritage structures under crowd-induced vibrations.

3.3. Implementation complexity

The implementation complexity varies substantially among the proposed strategies. The foam-based vibration-damping mat represents the simplest solution, requiring only temporary placement prior to the event; however, large-scale deployment requires careful logistical planning. The installation of geofoam barriers is moderately complex, as it requires excavation equipment and subsurface construction expertise, and may be constrained by existing underground utilities. The TMDI system presents the highest technical complexity, necessitating structural modifications, precise tuning, and potential architectural conflicts. This gradient of complexity directly influences the feasibility of each approach depending on the specific characteristics of the site.

3.4. Cost considerations

Cost differs markedly between solutions. Foam mats offer the lowest initial cost and can be reused, although replacement may be needed after a certain number of events due to material wear. Vibration-damping foam mats, as used in industrial and structural applications, typically cost about US $1–$12 per square foot (~US $10–$130 per m^2). Although per-unit material costs may appear modest, covering a large audience area can still lead to significant total expenditure, especially when higher performance materials are required (MQ Acoustic Materials). Geofoam barriers involve moderate installation costs but minimal maintenance, making them cost-effective over decades. Preliminary cost estimates from related ground vibration mitigation studies suggest initial installation costs for geofoam-filled trenches around ~€430 per unit, with lifecycle maintenance costs comparable to other subsurface solutions (Kaewunruen and Martin 2018). The TMDI system requires a high initial investment (design, fabrication,

installation) but has low operating costs, where it estimates TMD procurement and installation at around 2% of the total building construction cost (Tse, Kwok, and Tamura 2012). Lifecycle cost analysis suggests foam solutions are most economical for temporary events, while barriers and TMDI become competitive for permanent protection of high-value heritage assets subject to frequent anthropic excitations.

3.5. Compatibility with cultural heritage sites

The foam mat presents virtually no impact on existing structures since it is only a temporary and removable application, making it ideal for cultural heritage sites. Geofoam barriers require careful installation to minimize ground disturbance in archaeologically significant areas. The TMDI system poses the greatest heritage challenges, as installation requires structural modifications that may go against conservation principles. Compatibility often becomes the deciding factor in preservation projects, sometimes outweighing pure performance metrics.

3.6. Operational constraints

Practical operation during large events introduces additional considerations. Foam mats require storage and deployment before each event, potentially interfering with other operations. Geofoam barriers, once installed, function passively without operational requirements. The TMDI system operates continuously but may need occasional recalibration. Thus, the frequency of the events and site access limitations play crucial roles in strategy selection as frequent events may favour permanent solutions despite higher initial costs, while occasional events may better suit temporary measures.

4. Conclusions

This research directly addresses a critical gap, namely the need for effective solutions to protect historical masonry structures from low-frequency crowd-induced vibrations. Three vibration mitigation strategies, which are TMDI, foam-based vibration-damping mats, and subsoil geofoam barriers, are evaluated for vibration mitigation. By systematically comparing these three strategies using the Moletta Tower as a case study, this work provides a comprehensive framework tailored to heritage preservation.

The TMDI system provided moderate vibration control (10–40% reduction), proving effective when precisely tuned. The foam mat emerged as the most effective solution, reducing peak accelerations by up to 60% when using rubber foam, while composite EVA-rubber configurations maintained strong performance (55% reduction). Its non-invasive nature makes it particularly suitable for temporary events. Subsoil geofoam barriers demonstrated variable effectiveness (15–45% reduction), with deeper, more flexible barriers performing best, though their installation requires careful consideration of archaeological constraints. These findings advance the field by balancing engineering innovation with conservation priorities.

While this study provides valuable insights into vibration mitigation strategies for historic structures, certain limitations arise from inherent simplifications in the numerical modelling and the adopted assumptions. Firstly, the masonry was treated as a homogeneous material. In addition, the TMDI optimization relied on genetic algorithms to tune parameters based on a simplified SDOF representation of the tower's dominant mode. Furthermore, the effectiveness of the geofoam barriers was evaluated using a linear elastic wave-scattering approach, assuming small material deformations. Finally, the crowd-loading model, while incorporating synchronization effects, simplified human jumping dynamics as a uniform half-sinusoidal pulse.

These findings provide feasible solutions for safeguarding heritage structures in event-rich urban environments. The developed framework enables evidence-based selection of vibration mitigation strategies that balance heritage preservation requirements with contemporary use. The transferable methodology offers a template for protecting vibration-sensitive historic sites globally, advancing sustainable heritage conservation through interdisciplinary engineering approaches that reconcile structural performance with cultural significance.

Acknowledgement

The authors would like to thank Mauro Spampani and Alessandro Mitillo from Lunitek S.r.l (Italy) for providing the SHM sensors and their support in the data collection of the Moletta tower monitoring campaigns; the Capitoline Superintendent of Rome for their support during the Moletta tower monitoring campaigns.

Author contributions

CRediT: **Adel Bali:** Methodology, Software, Visualization, Writing – original draft; **Alessandro Cardoni:** Data curation, Supervision, Validation, Writing – review & editing; **Mohamed Abderaouf Louar:** Conceptualization, Investigation, Software, Supervision; **Gian Paolo Cimellaro:** Conceptualization, Funding acquisition, Methodology, Project administration, Resources, Supervision.

Disclosure statement

No potential conflict of interest was reported by the author(s).

References

Altan, M. 2018. "Thermoplastic Foams: Processing, Manufacturing, and Characterization." In *Recent Research in Polymerization*, edited by N. Cankaya, 236. UK: IntechOpen.

Alzawi, A., and M. H. El Naggar. 2011. "Full Scale Experimental Study on Vibration Scattering Using Open and In-Filled (GeoFoam) Wave Barriers." *Soil Dynamics and Earthquake Engineering* 31 (3): 306–317. https://doi.org/10.1016/j.soildyn.2010.08.010

Bachmann, H. 1995. *Vibration Problems in Structures: Practical Guidelines*. Basel, Switzerland: Birkhäuser Basel.

Bachmann, H., and W. Ammann. 1987. *Vibrations in Structures: Induced by Man and Machines*. Vol. 3. Zurich, Switzerland: International Association for Bridge and Structural Engineering.

Bertollucci Colherinhas, G., M. Morais, M. Shzu, and S. Avila. 2019. "Optimal Pendulum Tuned Mass Damper Design Applied to High Towers Using Genetic Algorithms: Two-DOF Modeling." *International Journal of Structural Stability and Dynamics* 19 (10): 1950125. https://doi.org/10.1142/S0219455419501256

Brancaleoni, R., F. Celletti, F. Garbin, G. Padula, L. Serio, and D. Spizzichino. 2015. "Consolidation and Restoration of the Moletta's Tower (Circus Maximus: Roma): Site Investigation and Monitoring." In *Engineering Geology for Society and Territory* -, edited by G. Lollino, D. Giordan, C. Marunteanu, B. Christaras, I. Yoshinori, and C. Margottini, 335–338. Vol. 8. Cham: Springer International Publishing. https://doi.org/10.1007/978-3-319-09408-3_58

Briody, C., B. Duignan, and S. Jerrams. 2011. "Characterisation, Modelling and Simulation of Flexible Polyurethane Foam."

Brown, C. P., T. C. Nguyen, H. R. Moody, R. W. Crawford, and A. Oloyede. 2009. "Assessment of Common Hyperelastic Constitutive Equations for Describing Normal and Osteoarthritic Articular Cartilage." *Proceedings of the Institution of Mechanical Engineers Part H, Journal of Engineering in Medicine* 223 (6): 643–652. Aug. https://doi.org/10.1243/09544119JEIM546

Carpentieri, E., D. De Rita, and G. D. Monica. 2015. "Geology of the Murcia Valley and Flood Plain Modifications in the Construction of the *Circus Maximus*, Rome, Italy." *Geoarchaeology* 30 (6): 483–494. Nov. https://doi.org/10.1002/gea.21533

Çelebi, E., S. Fırat, G. Beyhan, İ. Çankaya, İ. Vural, and O. Kırtel. 2009. "Field Experiments on Wave Propagation and Vibration Isolation by Using Wave Barriers." *Soil Dynamics and Earthquake Engineering* 29 (5): 824–833. https://doi.org/10.1016/j.soildyn.2008.08.007

CEN. 2005. *Eurocode 3: Design of steel structures. Part 1-1: General Rules and Rules for Buildings*. Brussels, Belgium: European Committee for Standardization. https://doi.org/10.1680/dsb.41721.011

Chen, J. 2016. *Human-Induced Load and Structural Vibration*. Beijing, China: Science Press.

Chen, R. Q., Z. Zhao, Y. Xia, C. Pan, H. Luo, and R. Zhang. 2019. "Comfort Based Floor Design Employing Tuned Inerter Mass System." *Journal of Sound and Vibration* 458:143–157. https://doi.org/10.1016/j.jsv.2019.06.019

Connor, J. J. 2003. *Introduction to Structural Motion Control*. New York, USA: Prentice Hall Pearson Education, Incorporated.

Coulier, P., V. Cuéllar, G. Degrande, and G. Lombaert. 2015. "Experimental and Numerical Evaluation of the Effectiveness of a Stiff Wave Barrier in the Soil." *Soil Dynamics and Earthquake Engineering* 77:238–253. https://doi.org/10.1016/j.soildyn.2015.04.007

De Angelis, M., A. Giaralis, F. Petrini, and D. Pietrosanti. 2019. "Optimal Tuning and Assessment of Inertial Dampers with Grounded Inerter for Vibration Control of Seismically Excited Base-Isolated Systems." *Engineering Structures* 196:109250. https://doi.org/10.1016/j.engstruct.2019.05.091

Djerouni, S., M. Abdeddaim, S. Elias, and R. Rupakhety. 2021. "Optimum Double Mass Tuned Damper Inerter for Control of Structure Subjected to Ground Motions." *Journal of Building Engineering* 44:103259. https://doi.org/10.1016/j.jobe.2021.103259

Ellis, B. R., and T. Ji. 2004. "The Response of Structures to Dynamic Crowd Loads." *Building Research Establishment*.

Fernández Martínez, J., L. Hermanns, A. Fraile De Lerma, and E. Alarcón Álvarez. 2016. "Jumping Load Models Applied on a Gymnasium Floor." *Engineering Structures* 125:26–38. Oct. https://doi.org/10.1016/j.engstruct.2016.06.051

Frahm, H. 1911. Device for Damping Vibrations of Bodies. U. S. Patent No. 989,958.

Gao, G., Q. Zhang, J. Chen, and Q. Chen. 2018. "Field Experiments and Numerical Analysis on the Ground Vibration Isolation of Wave Impeding Block Under Horizontal and Rocking Coupled Excitations." *Soil Dynamics and Earthquake Engineering* 115:507–512. https://doi.org/10.1016/j.soildyn.2018.09.015

Garrido, H., O. Curadelli, and D. Ambrosini. 2013. "Improvement of Tuned Mass Damper by Using Rotational Inertia Through Tuned Viscous Mass Damper." *Engineering Structures* 56:2149–2153. Nov. https://doi.org/10.1016/j.engstruct.2013.08.044

Gent, A. N. 2005. "Rubber Elasticity: Basic Concepts and Behavior." *Science and Technology of Rubber*: 1–27.

Guo, H., W. Hu, W. Guo, and R. Zou. 2015. "Constitutive Modeling of the Viscoelastic Mechanical Response of Foam Rubber-Like Materials." *RSC Advances* 5 (42): 33105–33113. https://doi.org/10.1039/C5RA03116H

'How much do damping materials cost? - Blog - MQ Acoustic Materials'. [Online]. https://www.mq-acoustics.com/blog/how-much-do-damping-materials-cost-1608493.html.

ISO 10137.2007. *Bases for Design of Structures–Serviceability of Buildings and Walkways Against Vibrations*. Geneva, Switzerland: International Organization for Standardization.

Jones, C. A., P. Reynolds, and A. Pavic. 2011. "Vibration Serviceability of Stadia Structures Subjected to Dynamic Crowd Loads: A Literature Review." *Journal of Sound and Vibration* 330 (8): 1531–1566. https://doi.org/10.1016/j.jsv.2010.10.032

Kaewunruen, S., and V. Martin. 2018. "Life Cycle Assessment of Railway Ground-Borne Noise and Vibration Mitigation

Methods Using Geosynthetics, Metamaterials and Ground Improvement." *Sustainability* 10 (10): 3753. Oct. https://doi.org/10.3390/su10103753

Kaewunruen, S., C. Ngamkhanong, M. Papaelias, and C. Roberts. 2018. "Wet/Dry Influence on Behaviors of Closed-Cell Polymeric Cross-Linked Foams Under Static, Dynamic and Impact Loads." *Construction and Building Materials* 187:1092–1102. https://doi.org/10.1016/j.conbuildmat.2018.08.052

Khaniki, H. B., M. H. Ghayesh, R. Chin, and M. Amabili. 2022. "A Review on the Nonlinear Dynamics of Hyperelastic Structures." *Nonlinear Dynamics* 110 (2): 963–994. https://doi.org/10.1007/s11071-022-07700-3

Kim, S., D. Lee, and S. Lee. 2024. "Optimal Design of Formulas for a Single Degree of Freedom Tuned Mass Damper Parameter Using a Genetic Algorithm and H2 Norm." *Biomimetics* 9 (8): 450. Aug. https://doi.org/10.3390/biomimetics9080450

Li, W., X. Yu, X. Hu, O. Tor, J. Zhang, T. Zhang, W. Qi, and L. Hu. 2023. "Finite Element Analysis of Compressive Stress-Strain Relations in Elastic Materials for Seat Foundation." *BioResources* 18 (4): 7731. https://doi.org/10.15376/biores.18.4.7731-7744

Li, Z., Q. Zhang, and F. Fan. 2022. "A Stochastic Approach for Generating Individual Jumping Loads Considering Different Jumping Force Patterns." *Journal of Building Engineering* 62:105378. Dec. https://doi.org/10.1016/j.jobe.2022.105378

Mahdavisefat, E., H. Salehzadeh, and A. A. Heshmati. 2018. "Full-Scale Experimental Study on Screening Effectiveness of SRM-Filled Trench Barriers." *Géotechnique* 68 (10): 869–882. https://doi.org/10.1680/jgeot.17.P.007

Massarsch, K. R. 2005. "Vibration Isolation Using Gas-Filled cushions." In *Geo-Frontiers*, Austin, Texas, January 24–26, 1–20. https://doi.org/10.1061/40780(159)7.

Matta, E. 2021. "Seismic Effectiveness and Robustness of Tuned Mass Dampers versus Nonlinear Energy Sinks in a Lifecycle Cost Perspective." *Bulletin of Earthquake Engineering* 19 (1): 513–551. Jan. https://doi.org/10.1007/s10518-020-00973-2

Mills, N. 2007. *Polymer Foams Handbook: Engineering and Biomechanics Applications and Design Guide*. Amsterdam, Netherlands: Elsevier. https://doi.org/10.1016/B978-0-7506-8069-1.X5000-4.

Mills, N. J. 2006. "Finite Element Models for the Viscoelasticity of Open-Cell Polyurethane Foam." *Cellular Polymers* 25 (5): 293–316. Sep. https://doi.org/10.1177/026248930602500502

Ministero delle Infrastrutture e dei Trasporti. 2018. *Norme tecniche per le costruzioni (NTC 2018)*.

Mirza Hessabi, R., and O. Mercan. 2016. "Investigations of the Application of Gyro-Mass Dampers with Various Types of Supplemental Dampers for Vibration Control of Building Structures." *Engineering Structures* 126:174–186. Nov. https://doi.org/10.1016/j.engstruct.2016.07.045

Moscatelli, M., S. Piscitelli, S. Piro, F. Stigliano, A. Giocoli, D. Zamuner, and F. Marconi. 2014. "Integrated Geological and Geophysical Investigations to Characterize the Anthropic Layer of the Palatine Hill and Roman Forum (Rome, Italy)." *Bulletin of Earthquake Engineering* 12 (3): 1319–1338. https://doi.org/10.1007/s10518-013-9460-5

Nadeau, B. L. "'A Miracle and a Warning: Ancient Tower Collapse Reveals a Crisis Facing Modern Rome'." CNN. [Online]. Available: https://www.cnn.com/2025/11/25/travel/torre-dei-conti-collapse-rome-future.

Nikooyan, A. A., and A. A. Zadpoor. 2011. "Mass–Spring–Damper Modelling of the Human Body to Study Running and Hopping – an Overview." *Proceedings of the Institution of Mechanical Engineers Part H, Journal of Engineering in Medicine* 225 (12): 1121–1135. Dec. https://doi.org/10.1177/0954411911424210

Puzzilli, L. M., G. Bongiovanni, P. Clemente, V. Di Fiore, and V. Verrubbi. 2021. "Effects of Anthropic and Ambient Vibrations on Archaeological Sites: The Case of the Circus Maximus in Rome." *Geosciences* 11 (11): 463. https://doi.org/10.3390/geosciences11110463

Racic, V., A. Pavic, and J. M. W. Brownjohn. 2009. "Experimental Identification and Analytical Modelling of Human Walking Forces: Literature Review." *Journal of Sound and Vibration* 326 (1–2): 1–49. https://doi.org/10.1016/j.jsv.2009.04.020

Richart, F. E., J. R. Hall, and R. D. Woods. 1970. "Vibrations of Soils and Foundations."

Sadeghnejad, S., Y. Taraz Jamshidi, R. Mirzaeifar, and M. Sadighi. 2019. "Modeling, Characterization and Parametric Identification of Low Velocity Impact Behavior of Time-Dependent Hyper-Viscoelastic Sandwich Panels." *Proceedings of the Institution of Mechanical Engineers, Part L: Journal of Materials: Design and Applications* 233 (4): 622–636. Apr. https://doi.org/10.1177/1464420716688233

Sim, J., A. Blakeborough, M. S. Williams, and G. Parkhouse. 2008. "Statistical Model of Crowd Jumping Loads." *Journal of Structural Engineering* 134 (12): 1852–1861. Dec. https://doi.org/10.1061/(ASCE)0733-9445(2008)134:12(1852)

Su, J., and Y. Wang. 2013. "Equivalent Dynamic Infinite Element for Soil–Structure Interaction." *Finite Elements in Analysis and Design* 63:1–7. Jan. https://doi.org/10.1016/j.finel.2012.08.006

Suryadi, D., A. Prasetya, N. Daratha, and I. Agustian. 2023. "Optimum Design Of Tuned Mass Damper Parameters To Reduce Seismic Response On Structure Using Genetic Algorithm." *ASEAN Engineering Journal* 13 (1): 41–49. Feb. https://doi.org/10.11113/aej.v13.17890

Tapia Romero, M. A., M. Dehonor Gomez, and L. E. Lugo Uribe. 2020. "Prony Series Calculation for Viscoelastic Behavior Modeling of Structural Adhesives from DMA Data." *Ingeniería Investigación y Tecnología* 21 (2): 1–10. Apr. https://doi.org/10.22201/fi.25940732e.2020.21n2.014

TMD (China Tuned Mass Damper). "Manufacturers Suppliers - Customized Tuned Mass Damper (TMD) - Luze New Materials."

Tomin, M., and Á. Kmetty. 2022. "Polymer Foams as Advanced Energy Absorbing Materials for Sports applications—A Review." *Journal of Applied Polymer Science* 139 (9): 51714. https://doi.org/10.1002/app.51714

Tse, K. T., K. C. S. Kwok, and Y. Tamura. 2012. "Performance and Cost Evaluation of a Smart Tuned Mass Damper for Suppressing Wind-Induced Lateral-Torsional Motion of Tall Structures." *Journal of Structural Engineering* 138 (4): 514–525. Mar. https://doi.org/10.1061/(ASCE)ST.1943-541X.0000486

UNI 9916. 2004. Criteri di misura e valutazione degli effetti delle vibrazioni sugli edifici. Milan, Italy: Ente Italiano di Normazione.

White, S. W. 1998. "'Dynamic Modeling and Measurement of Occupied Car Seats and Seating foam', Master's Thesis, West Lafayette, IN: School of Mechanical Engineering, Purdue University, 47907.

Woods, R. D. 1968. "Screening of Surface Wave in Soils." *Journal of the Soil Mechanics and Foundations Division* 94 (4): 951–979. Apr. https://doi.org/10.1061/JSFEAQ.0001180

Wu, J., F. Lu, J. Chen, and M. Wang. 2023. "A One-Dimensional Dynamic Constitutive Modeling of Ethylene Vinyl Acetate (EVA) Foam." *Polymers* 15 (23): 4514. https://doi.org/10.3390/polym15234514

Yang, F., R. Sedaghati, and E. Esmailzadeh. 2022. "Vibration Suppression of Structures Using Tuned Mass Damper Technology: A State-Of-The-Art Review." *Journal of Vibration and Control* 28 (7–8): 812–836. Apr. https://doi.org/10.1177/1077546320984305

Zhang, T., W. Wang, X. Li, and B. Wang. 2023. "Vibration Mitigation in Offshore Wind Turbine Under Combined Wind-Wave-Earthquake Loads Using the Tuned Mass Damper Inerter." *Renewable Energy* 216:119050. https://doi.org/10.1016/j.renene.2023.119050

Zhou, G., and R. K. L. Su. 2023. "A Review on Durability of Foam Concrete." *Buildings* 13 (7): 1880. Jul. https://doi.org/10.3390/buildings13071880

Zhu, H. X., and N. J. Mills. 1999. "Modelling the Creep of Open-Cell Polymer Foams." *Journal of the Mechanics and Physics of Solids* 47 (7): 1437–1457. Jun. https://doi.org/10.1016/S0022-5096(98)00116-1

Zilletti, M., S. J. Elliott, and E. Rustighi. 2012. "Optimisation of Dynamic Vibration Absorbers to Minimise Kinetic Energy and Maximise Internal Power Dissipation." *Journal of Sound and Vibration* 331 (18): 4093–4100. https://doi.org/10.1016/j.jsv.2012.04.023